KERNFORSCHUNGSZENTRUM

KARLSRUHE

November 1970

KFK 1364

Institut für Experimentelle Kernphysik

The Angular Distribution of Final State Interacting n-p Pairs in the Reaction p+d → p+p+n

H. Brückmann, W. Kluge, H. Matthäy, L. Schänzler, K. Wick

GESELLSCHAFT FÜR KERNFORSCHUNG M. B. H.

KARLSRUHE

1.B

Nuclear Physics A157 (1970) 209—230; © *North-Holland Publishing Co., Amsterdam*

THE ANGULAR DISTRIBUTION OF FINAL STATE INTERACTING n-p PAIRS IN THE REACTION p+d → p+p+n

H. BRÜCKMANN, W. KLUGE, H. MATTHÄY, L. SCHÄNZLER and K. WICK

Institut für Experimentelle Kernphysik des Kernforschungszentrums und der Universität Karlsruhe

Received 6 July 1970

Abstract: The three-particle reaction p+d → p+p+n has been investigated systematically at a deuteron bombarding energy of 52.3 MeV. Kinematically complete experiments have been carried out by detecting the two protons in coincidence. The kinematical conditions were chosen predominantly to observe the effect of the n–p final state interaction. All the data are analysed in terms of the Watson-Migdal model of final state interactions. At specific kinematical conditions the impulse approximation turns out to be a more general and better description.

An angular distribution was obtained for the production of singlet and triplet final state interacting n–p pairs with zero relative energy in the n–p subsystem. A relation is derived which connects the measured angular distribution for triplet final state interaction in the three-nucleon reaction quantitatively with the angular distribution of elastic p–d scattering.

The systematic study proves that values of the nucleon-nucleon scattering lengths can be extracted with a high degree of reliability from three-particle reactions under properly chosen kinematical conditions.

E

NUCLEAR REACTIONS ^{1}H(d, 2p), $E = 52.3$ MeV; measured $\sigma(E_{p1}, \theta_1, E_{p2}, \theta_2)$; deduced $\sigma(\theta)$ for production of n–p pairs with zero relative energy ($E_{np} = 0$) in singlet and triplet state n–p singlet scattering length a^s.

1. Introduction

In recent years in nuclear physics considerable effort has been concentrated on the experimental and theoretical investigation of few-body problems. Within this field particular interest is paid to the study of the simplest nuclear reactions p+d → p+p+n and n+d → p+n+n involving three nucleons only. There are two main relevant questions to be answered by a systematic investigation of these two reactions.

Firstly one aims at a complete understanding of the reaction mechanism responsible for such a three-nucleon break-up. Therefore one is interested in the limits of applicability of special reaction models.

Secondly one wants to determine how to extract properties of the two-nucleon interaction from a three-nucleon reaction. The answer to this question is particularly needed for the determination of neutron-neutron scattering parameters. At laboratory conditions the n-n interaction can be studied only in three-particle reactions like n+d → p+n+n [see refs. [1–3])]. Prior to the extraction of reliable n-n scattering parameters the limits of applicability of the final state interaction model have to be determined. For this purpose the n-p scattering parameters extracted from the n-p

final state interaction have to be compared with the values well known from free n-p scattering. Although such a comparison can be carried out in the reaction n+d → p+n+n it is more convenient from the experimental point of view to investigate the reaction p+d → p+p+n.

A complete theoretical description of a three-particle reaction has to be based on calculations which solve the many-body problem by using only the knowledge of the nucleon-nucleon forces. From the point of view of a formal scattering theory the three-body problem is to be regarded as principally solved [see e.g. refs. [4-12])]. Numerical calculations however require such extremely large computer capacities that approximations have to be used. Only a few authors have presented numerical results which can be compared directly with the experimental data [see e.g. refs. [9,11,12])].

The experimental data available in the literature for the reaction p+d → p+p+n contain to a considerable extent results based on single counter experiments where only one of the outgoing particles was detected [kinematically incomplete experiments, see e.g. refs. [13,14])]. Only a small number of groups reported coincidence experiments which are kinematically complete [1,15-31]). Almost none of the experiments published up to now covered the effects of final state interaction systematically in a very broad kinematical region. This is partly due to the fact that in general protons have been used as projectiles and in this case the quasielastic scattering process can be observed more conveniently.

The systematic study of the reaction p+d → p+p+n was carried out by means of coincidence experiments in a wide region of kinematics at a deuteron bombarding energy of 52 MeV. The general aims of our whole set of experiments were

(i) to measure an angular distribution for the production of final state interacting neutron-proton singlet and triplet pairs;

(ii) to check the applicability of the Watson-Migdal model [32,33]) of final state interaction (FSI) at many different kinematical conditions;

(iii) to check the validity of the two-step reaction model by measuring the angular distribution in the neutron-proton c.m. subsystem;

(iv) to investigate the proton-proton FSI down to very low relative energies where free p-p scattering cannot be studied experimentally;

(v) to compare the neutron-proton FSI with the proton-proton FSI at identical kinematical conditions.

The present paper deals with the neutron-proton final state interaction only and covers the topics (i) and (ii). The results obtained on topics (iii)–(v) will be discussed separately.

2. Experimental procedure

The focussed 52.3 MeV deuteron beam of the Karlsruhe isochronous cyclotron was used to bombard a polyethylene target. The set-up is shown schematically in fig. 1. Two NaI(Tl) scintillation detectors placed at angles θ_3 and θ_4 were used to

detect the two protons in coincidence. Distances between target and detectors of up to 120 cm allowed an excellent angular resolution of 0.3–0.5° typically. Such large distances also allowed the particle identification to be made by time-of-flight technique [ref. [34])]. An energy signal E and a timing signal t was derived from each detector. The timing signals t and reference pulses from the cyclotron RF were fed into special electronic circuits which deliver two time-of-flight signals. The detailed features of

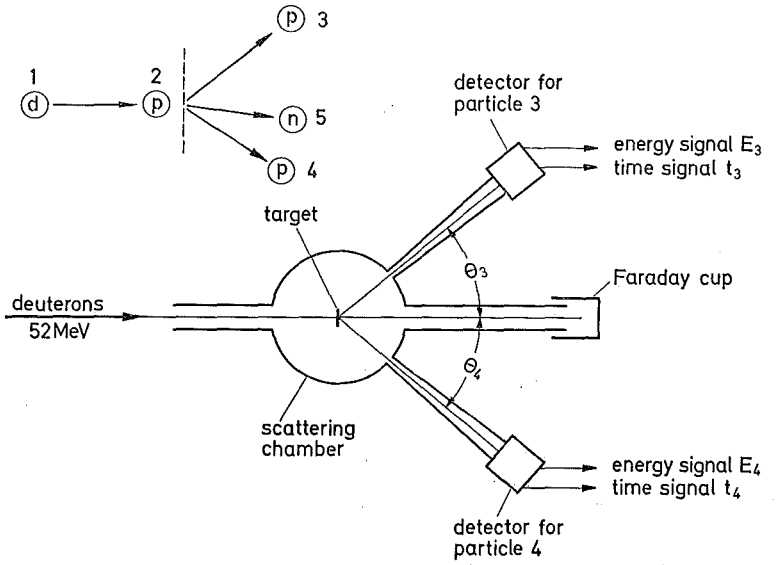

Fig. 1. The experimental set-up and the nomenclature used for the particles and angles.

this electronic system are described in ref. [34]). The two energy signals and the two time-of-flight signals were fed into a data acquisition system (DATA) [35]) being connected on-line to a CDC 3100 computer. The whole information on each coincidence event was assembled in one or two 24-bit computer words and recorded on magnetic tape. The final data processing was carried out with an IBM 360/65 computer. The details of the experimental set-up and the electronic data processing are described elsewhere [27,34,35]).

The total charge of the incident beam was measured with a Faraday cup and a current integrator. In order to be independent of changes in target thickness with time and from errors in the charge measurement an additional monitor detector was placed at a fixed angle. The spectrum of the monitor was registered separately.

3. The neutron-proton final state interaction in the reaction p+d → p+p+n

3.1. AN EXAMPLE OF EXPERIMENTAL DATA AND THE METHODS OF ANALYSIS

The n-p final state interaction was investigated in the reaction

$$p+d \rightarrow p+p+n,$$

(denoted in the following as particles $1+2 \rightarrow 3+4+5$) by observation of coincidences between the two outgoing protons. The proton energies are denoted by E_3 and E_4. At fixed angles θ_3 and θ_4 the energies of the two protons are correlated by the kinematics and all the coincidence events are located on a kinematically allowed curve in the E_3–E_4 plane [27,36]).

In general several different reaction mechanisms are contributing in a rather complex way to the three-particle cross section. An advantage of kinematically complete experiments is that a proper choice of the pair of angles allows the reaction to be observed at kinematical conditions where one reaction mechanism is dominating. For instance at small relative energies E_{np} (e.g. E_{35} or E_{45}) one expects the n–p final state

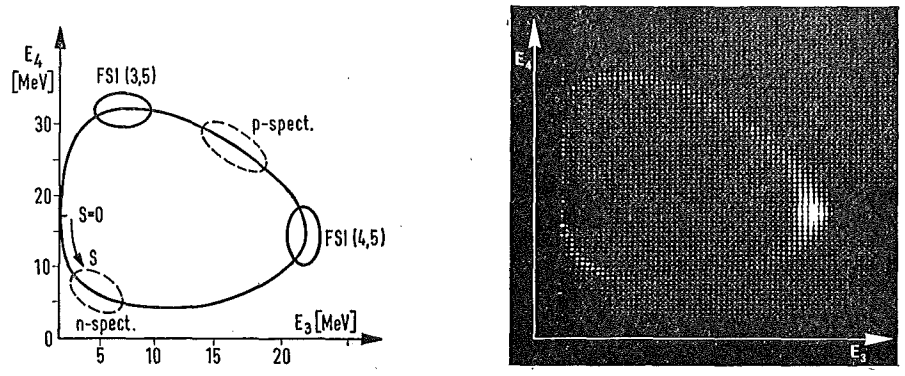

Fig. 2. a) Kinematics of the reaction p+d → p+p+n at 52.3 MeV deuteron bombarding energy. The kinematically allowed curve is shown in the E_3–E_4 plane for angles $\theta_3 = 42.0°$ and $\theta_4 = 25.3°$. Regions where final state interaction is expected are denoted by FSI. In quasielastic scattering a proton might be the spectator particle (p–spect.) or the neutron does not participate in the reaction (n–spect.). S denotes the arc length along the kinematical urve [see eq. (1)]. b) The corresponding experimental data shown as a map display in an array of 64–64 channels.

interaction to be dominant. Therefore one wants E_{np} to reach down to zero along the kinematically allowed curve. This condition fixes θ_4 after θ_3 is chosen or vice versa [refs. [27,36])]. Fig. 2a shows as an example the kinematically allowed curve for the set of angles $\theta_3 = 42.0°$ and $\theta_4 = 25.3°$. At fixed angles θ_3 and θ_4 the relative energy E_{45} is a single valued function of the energy E_3. A corresponding relation holds also for E_{35} and E_4 [refs. [27,36])]. The energies E_{45} or E_{35} have their minimum values at the points where E_3 or E_4 respectively have their maximum. This special feature of the kinematics leads to a very slow variation of the relative energies in the neighbourhood of these extrema. This phenomenon of "kinematical amplification" can be observed in kinematically complete experiments only.

The main contribution of the FSI between the proton 3 and the neutron 5 will appear in the region labelled in fig. 2a as FSI (3, 5). The n–p FSI of the (4, 5) pair will be observed predominantly in the region FSI (4, 5). In the example of fig. 2a only the energy E_{45} becomes zero and thus a particular large FSI contribution is expected

at FSI (4, 5) only. The minimum for the energy E_{35} is 1.15 MeV and the FSI contribution from the singlet state interaction of the particles 3 and 5 is expected to be very small †.

In a quasielastic scattering [23,37]) either the neutron or the proton of the projectile deuteron can act as a spectator particle. If the neutron is taken to be the spectator the main contribution of the spectator effect will be observed in the region labelled as "n-spect". If the proton however acts as a spectator an enhancement of events will be found in the region denoted by "p-spect". In the example of fig. 2a a proton spectator has to carry off a rather high momentum from the internal momentum distribution in the deuteron and hence the effect of quasielastic scattering can be neglected. At

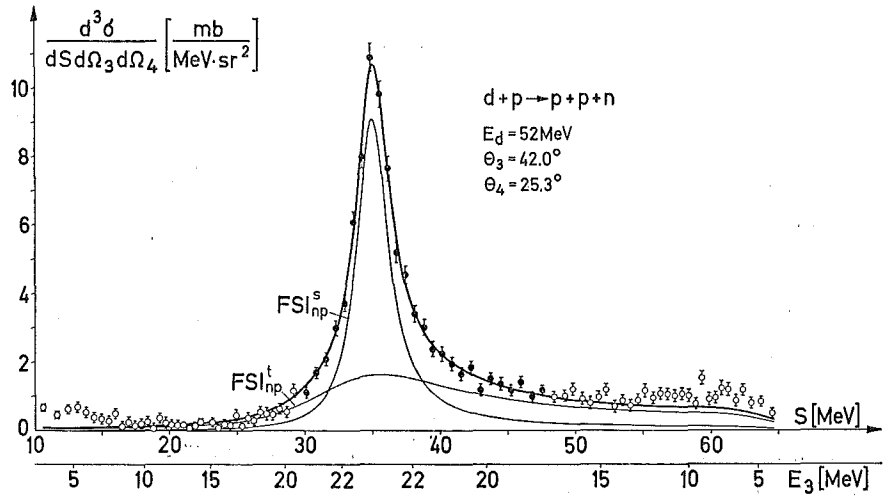

Fig. 3. The three-particle cross section of the reaction d+p → p+p+n plotted versus the arc length S and E_3 the proton energy. The solid curve is the result of an analysis based on formula (5). The contributions from n–p FSI in singlet state (FSI_{np}^{s}) an n–p FSI in triplet state (FSI_{np}^{t}) are shown separately.

these kinematical conditions one expects the investigation of the n–p FSI between the particles 4 and 5 to be possible with only negligible distortions from other reaction mechanisms.

The corresponding experimental data are shown in the map display of fig. 2b in an array of 64×64 channels. The special experimental arrangement in use allows the registration even of coincidence events where one particle has a very low energy. As is seen from the map display the whole kinematical curve is populated by coincidence events. The FSI enhances the cross section strongly at high values of the energy E_3 and a FSI peak is clearly visible. Random coincidences have been subtracted as discussed in ref. [35]). For the analysis of the data the number of coincidence events is

† The contribution of triplet FSI in the n–p pair (3, 5) is negligible because the particular pair of angles corresponds to the minimum in the angular distribution of triplet FSI (see fig. 7).

projected onto the kinematical curve of fig. 2a. The position on the kinematical curve is characterized by the arc length S as indicated in fig. 2a.

The arc length S is defined in ref. [36]) by the equation

$$S = \int \sqrt{(\mathrm{d}E_3)^2+(\mathrm{d}E_4)^2}. \tag{1}$$

Fig. 3 shows the experimentally obtained three-particle cross section plotted versus the arc length S and E_3 the proton energy. The methods used to analyse the measured three-particle cross section is to be described briefly.

The three-particle cross section is given by

$$\frac{\mathrm{d}^3\sigma}{\mathrm{d}S\,\mathrm{d}\Omega_3\,\mathrm{d}\Omega_4} = \frac{2\pi}{\hbar}\frac{m_1}{p_1}|T_{\mathrm{fi}}|^2\rho_{\mathrm{S}}(E_3, E_4), \tag{2}$$

where T_{fi} is the three-particle transition matrix element, ρ_{S} is the phase space factor [ref. [36])], m_1 and p_1 are the mass and the momentum of the projectile deuteron. Assuming a two-step reaction mechanism the squared three-particle reaction matrix element $|T_{\mathrm{fi}}|^2$ can be written according to Goldberger and Watson [32,38]) as

$$|T_{\mathrm{fi}}|^2 = F_{\mathrm{np}}(E_{\mathrm{np}})|T^0_{\mathrm{fi}}|^2, \tag{3}$$

where F_{np} is the enhancement factor for the n–p FSI and T^0_{fi} is the matrix element for the production of the final state interacting n–p pair. According to Watson T^0_{fi} should depend only very weakly on the relative energy E_{np} and hence the variation of T^0_{fi} with E_{np} is neglected. The n–p pair can be produced in the singlet or in the triplet state. Therefore two enhancement factors $F^{\mathrm{s}}_{\mathrm{np}}$ and $F^{\mathrm{t}}_{\mathrm{np}}$ have to be used [28]).

Both factors are written in the following form

$$F_{\mathrm{np}} = \frac{(\kappa^2+\alpha^2)^2\frac{1}{4}r_0^2}{\left(-\frac{1}{a}+\frac{r_0}{2}\kappa^2\right)^2+\kappa^2}. \tag{4a}$$

As defined in ref. [38]) α is given by

$$\alpha = \frac{1}{r_0}(1+\sqrt{1-2r_0/a}) \tag{4b}$$

and $\kappa = (ME_{\mathrm{np}}/\hbar^2)^{\frac{1}{2}}$ is the momentum of the neutron and the proton in the c.m. of the n–p pair, M is the mass of a nucleon, a is the scattering length, r_0 the effective range. Accounting for the final state interaction of one n–p pair only, e.g. the pair (4, 5), and assuming an incoherent superposition of the singlet and triplet amplitudes the cross section is written as the sum

$$\frac{\mathrm{d}^3\sigma}{\mathrm{d}S\,\mathrm{d}\Omega_3\,\mathrm{d}\Omega_4} = \mathrm{FSI}^{\mathrm{s}}_{\mathrm{np}}+\mathrm{FSI}^{\mathrm{t}}_{\mathrm{np}} = [X^{\mathrm{s}}_{\mathrm{np}}(\theta_3)F^{\mathrm{s}}_{\mathrm{np}}(E_{45})+X^{\mathrm{t}}_{\mathrm{np}}(\theta_3)F^{\mathrm{t}}_{\mathrm{np}}(E_{45})]\rho_{\mathrm{S}}(E_3, E_4), \tag{5}$$

where e.g. $X^{s}_{np}(\theta_3)$ is given by

$$X^{s}_{np}(\theta_3) = \frac{2\pi}{\hbar}\,\frac{m_1}{p_1}\,|T^{0}_{fi}|^2_{singlet}, \tag{6}$$

X^{s}_{np} and X^{t}_{np} are factors which are proportional to the production probability of the n–p subsystem in the singlet and triplet state.

The expression (5) is used to determine the three parameters a^s the singlet scattering length and the production probabilities, X^{s}_{np} and X^{t}_{np} by least-square fit calculations. (The FSI(4, 5) dominates in the region denoted by full dots in fig. 3. Only these data were used in the least-square fit calculations.) The analysis turns out to be insensitive to a variation of the parameters a^t the triplet scattering length, r^s the singlet effective range and r^t the triplet effective range. For these parameters the values known from free n–p scattering were therefore inserted:

$$a^t = 5.41 \pm 0.01 \quad \text{fm},$$
$$r^s = 2.67 \pm 0.02 \quad \text{fm},$$
$$r^t = 1.750 \pm 0.015 \text{ fm}.$$

The curves in the example of fig. 3 represent the result of least-square fit calculations including the effects of angular resolution and finite target thickness. Obviously the experimental data can be fitted excellently along the whole kinematical curve by expression (5). Small differences arise only at very low and very high values of the arc length S.

As pointed out above one expects other reaction mechanisms to contribute in these regions. But in the example discussed here these contributions are seen to be negligible, at least they can be completely neglected in the region of dominating FSI. Hence this example is an appropriate one to determine a reliable value of the singlet scattering length a^s if the Watson formula holds. The result obtained is $a^s = -23.2 \pm 0.6$ fm which is to be compared with the value known from free n–p scattering $a^{s}_{free} = -23.68 \pm 0.03$ fm [ref. [39])]. The example discussed above shows that the Watson-Migdal theory is very adequate to describe the cross section as long as one chooses kinematical conditions where the contributions from other competing reaction mechanisms are negligible.

3.2. THE ANGULAR DISTRIBUTION OF THE REACTION p(d, d*)p

3.2.1. *Experimental results.* Coincidence experiments of the kind as illustrated in the preceding section have been carried out at ten different pairs of angles. The aim was to measure angular distributions for the production of the n–p subsystem (d*) in the singlet and the triplet state. As is pointed out in subsect. 3.1 the d* production cross section is expected to have a maximum at a relative energy $E_{np} = 0$. Hence all pairs of angles were chosen in such a way that the corresponding kinematical curve contains at least one point where E_{np} is zero.

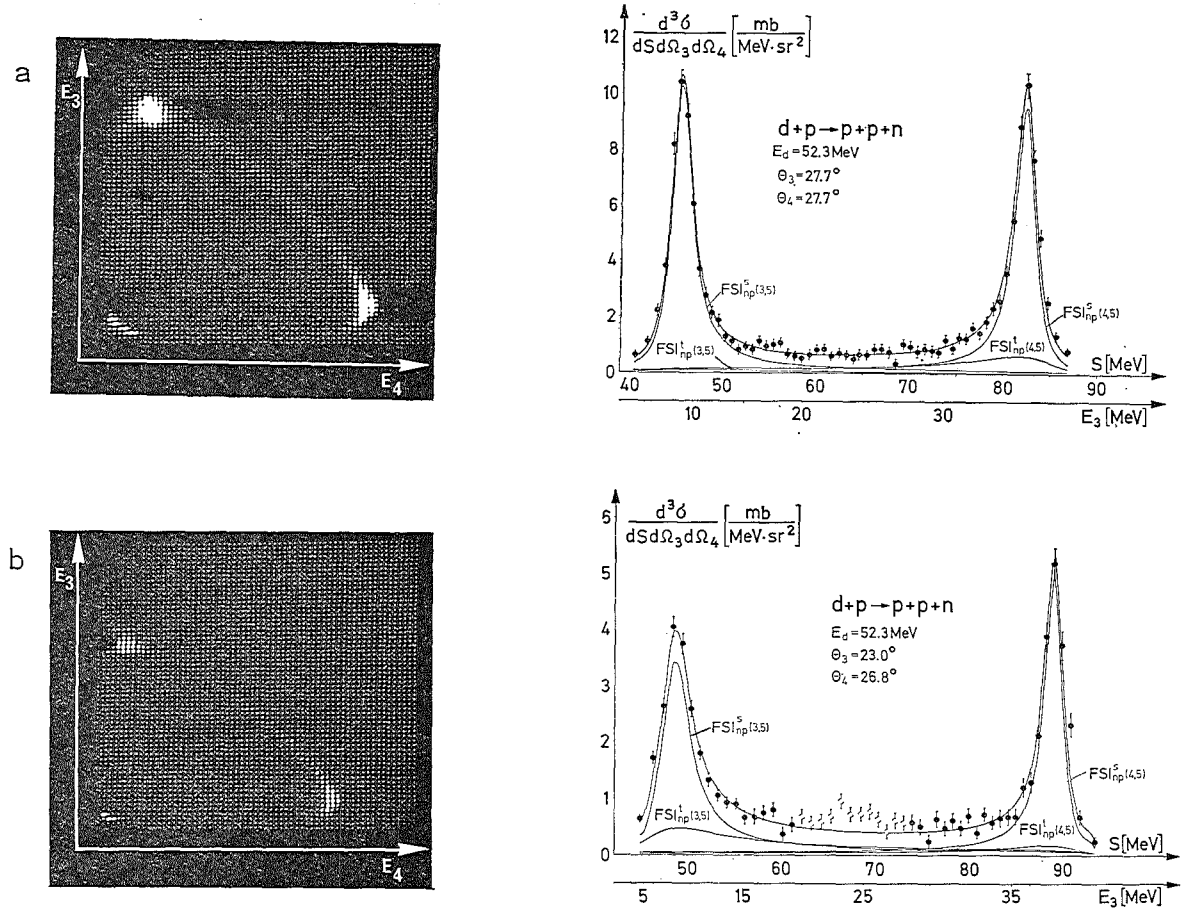

Fig. 4. a) Experimental map display and the corresponding coincidence spectrum for the unique situation where two identical FSI peaks ($E_{np} = 0$) arise $\theta_3 = \theta_4 = 27.7°$. b) Data taken at the angles $\theta_3 = 23.0°$ and $\theta_4 = 26.8°$.

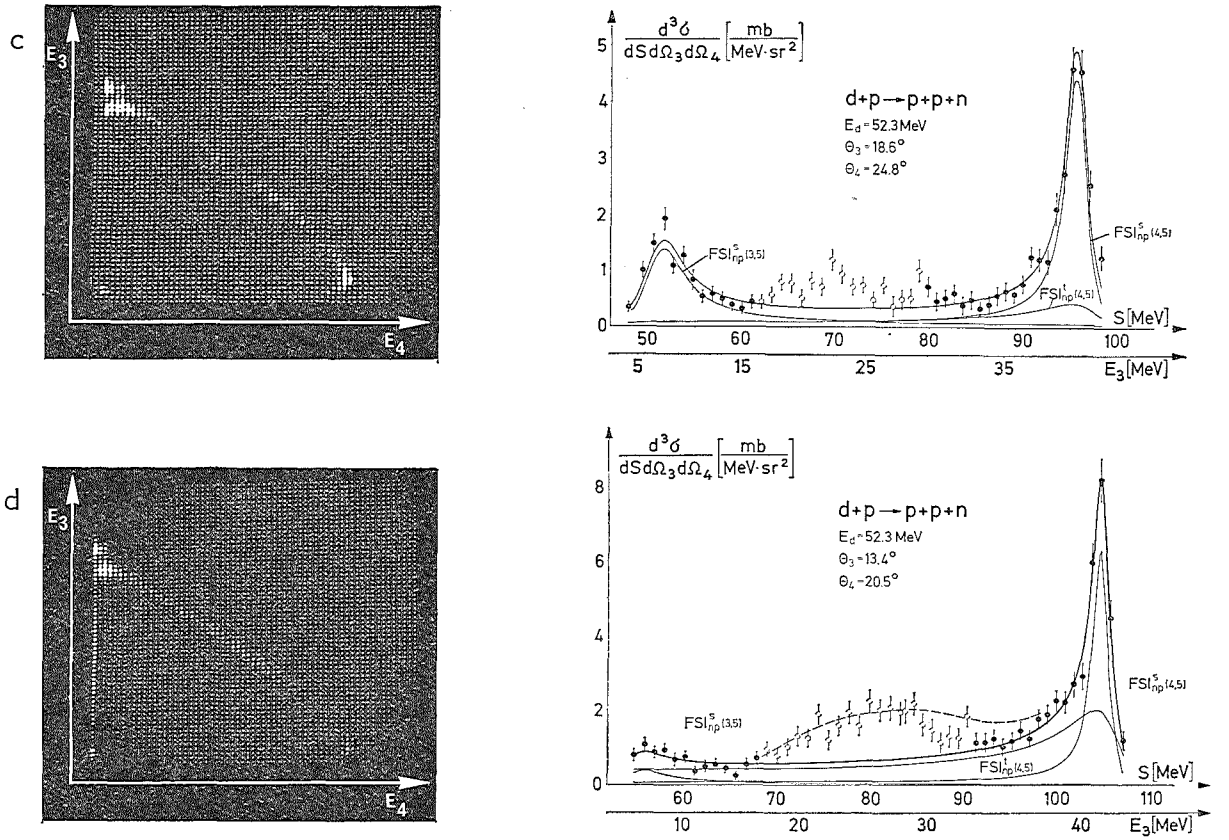

Fig. 4. c) Data taken at the angles $\theta_3 = 18.6°$ and $\theta_4 = 24.8°$. d) Data taken at the angles $\theta_3 = 13.4°$ and $\theta_4 = 20.5°$.

Figs. 4a–d show some of the map displays and the corresponding coincidence spectra. The spectra are presented as a function of the arc length S and the proton energy E_3. Fig. 4a represents the unique situation where n–p pairs with zero relative energy can be observed at two different points of the kinematical curve. The angles for this unique situation are $\theta_3 = \theta_4 = 27.7°$. The neutron can form a zero energy n–p system with each of the two protons. Two identical FSI peaks arise from these two n–p pairs. The pairs are denoted as (3, 5) and (4, 5) couples.

Contrary to fig. 2 the figs. 4b–d show examples where pairs of angles in the vicinity of the unique symmetrical position have been chosen. Although two FSI peaks can be seen E_{np} becomes zero only at one of the peaks. The kinematical situation is quite different from the situation of the example shown in fig. 2.

Analysing these spectra one has to account for the FSI of both n–p pairs. The expression (5) for the three-particle cross section is replaced by

$$\begin{aligned}\frac{\mathrm{d}^3\sigma}{\mathrm{d}S\,\mathrm{d}\Omega_3\,\mathrm{d}\Omega_4} &= \mathrm{FSI}^{\mathrm{s}}_{\mathrm{np}}(4,5)+\mathrm{FSI}^{\mathrm{t}}_{\mathrm{np}}(4,5)+\mathrm{FSI}^{\mathrm{s}}_{\mathrm{np}}(3,5)+\mathrm{FSI}^{\mathrm{t}}_{\mathrm{np}}(3,5)\\ &= [X^{\mathrm{s}}_{\mathrm{np}}(\theta_3)F^{\mathrm{s}}_{\mathrm{np}}(E_{45})+X^{\mathrm{t}}_{\mathrm{np}}(\theta_3)F^{\mathrm{t}}_{\mathrm{np}}(E_{45})+X^{\mathrm{s}}_{\mathrm{np}}(\theta_4)F^{\mathrm{s}}_{\mathrm{np}}(E_{35})\\ &\quad + X^{\mathrm{t}}_{\mathrm{np}}(\theta_4)F^{\mathrm{t}}_{\mathrm{np}}(E_{35})]\rho_{\mathrm{S}}(E_3, E_4). \qquad (7)\end{aligned}$$

Interferences between the (3, 5) and (4, 5) FSI amplitudes have been neglected.

The n–p pairs (3, 5) and (4, 5) are produced at different angles and therefore five independent parameters are determined from each spectrum. These parameters are a^{s}, $X^{\mathrm{s}}_{\mathrm{np}}(\theta_3)$, $X^{\mathrm{s}}_{\mathrm{np}}(\theta_4)$, $X^{\mathrm{t}}_{\mathrm{np}}(\theta_3)$ and $X^{\mathrm{t}}_{\mathrm{np}}(\theta_4)$. They were determined by least-squares fit calculations from the fraction of the data which is plotted by full dots. The results of the calculations are represented by the full curves in figs. 4a–d.

In the symmetrical situation (fig. 4a) the experimental data are fitted excellently by the calculated curves. The FSI ansatz used turns out to be adequate to reproduce all the data in this kinematical region. Other reaction mechanisms are not interfering. At angles which are only approximately symmetrical the experimental data are not adequately reproduced. With decreasing angles θ_3 and θ_4 one observes increasing disagreement with the FSI calculations (regions where the data are plotted by open circles). This disagreement results from an increasing contribution of the quasielastic scattering at forward angles θ_3 and θ_4.

A more detailed theoretical treatment is required for an interpretation of the data shown in figs. 4b–d. According to Gluckstern and Bethe [40]) and Gammel *et al.* [41,42]) in first order Born approximation six graphs must be considered for the p–d reaction.

The graphs in fig. 5a describe the first reaction step as a quasielastic scattering between the free proton and one of the nucleons in the deuteron. The second step accounts for the final state interaction. The graphs (fig. 5a) contain neutron-proton FSI only. This restriction is a good approximation for low relative neutron-proton energies E_{35} and E_{45}. In this case the relative energy of the two protons $E_{\mathrm{pp}} = E_{34}$ is so large that contributions of a proton-proton FSI can be neglected.

The contributions from the different graphs to the cross section are strongly dependent on the c.m. emission angle θ_{d^*} of the low-energy neutron-proton pair. This dependence is shown qualitatively in fig. 5b. At large angles the graphs $J_2^{\pm}$ are dominating. Therefore one might attempt to explain the data taken at large c.m. angles θ_{d^*} with the graphs $J_2^{\pm}$ only ($\theta_{d^*} > 140°$).

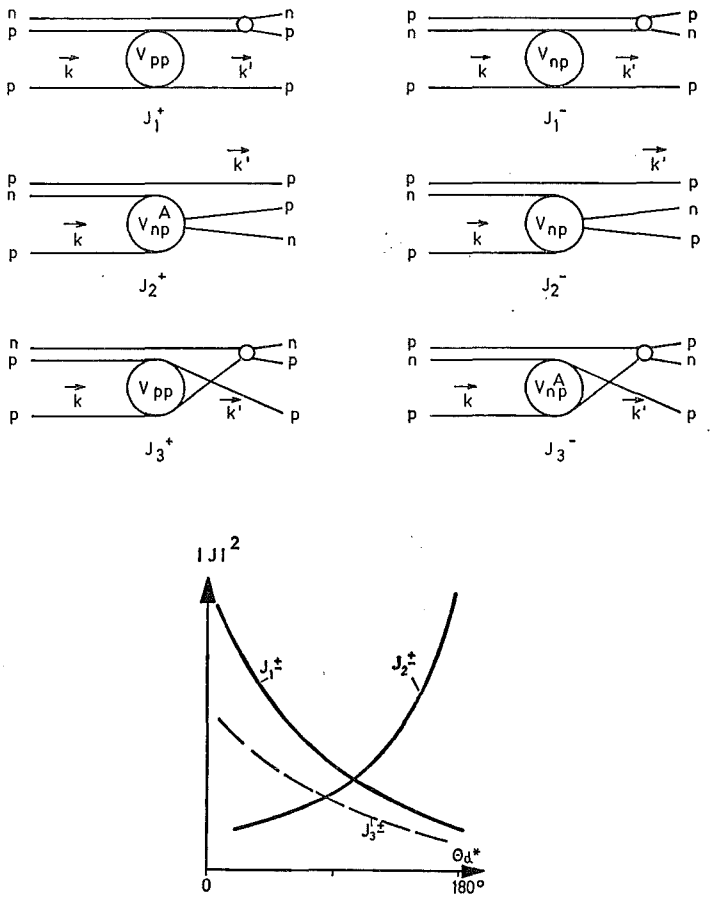

Fig. 5. a) The six basic graphs for the p–d reaction in the first order Born approximation. The first step is assumed to be a quasielastic proton-nucleon scattering. In the second step only n–p FSI is taken into account. b) The contributions of the different graphs are shown qualitatively as a function of the c.m. emission angle θ_{d^*} of the final state interacting n–p pair.

The graph $J_2^{\pm}$ is a specific one in the sense that the FSI is already included in the first step. Therefore the graph $J_2^{\pm}$ describes the reaction mechanism in terms of a quasielastic neutron-proton scattering only. Consequently it is more suitable in this specific case to treat the quasielastic n–p scattering in terms of the impulse approxi-

mation [23,37]). In the impulse approximation the cross section is given by

$$\frac{d^3\sigma}{d\Omega_3\, d\Omega_4\, dS} = \text{const.}|\psi_d(k_3^i)|^2 \left(\frac{d\sigma}{d\Omega}\right)_{np} \rho_S, \tag{8}$$

where k_3^i is the internal momentum of the spectator proton (particle 3) in the deuteron, $|\psi_d|^2$ is the Fourier transform of the deuteron wave function and $(d\sigma/d\Omega)_{np}$ is the off-energy shell cross section for n–p scattering (particles 4 and 5). Conveniently $(d\sigma/d\Omega)_{np}$ is replaced by the on-shell neutron-proton cross section taken at the relative energy $E_{np} = E_{45}$ of the final state interacting n–p pair.

TABLE 1
Numerical results of the analysis

θ_3[°]/θ_4[°]	θ_{d*}	a^s[fm]	σ^s[mb/MeV · sr²] for $E_{np} = 0$	σ^t[mb/MeV · sr²] for $E_{np} = 0$
13.4/20.5	152.0	$-21.0^{+1.0}_{-2.0}$	7.3±0.7	2.0 ±0.3
18.6/24.8	141.0	−15.9±2.0	5.0±0.5	0.40±0.15
23.0/26.8	131.8	−20.2±1.5	5.4±0.5	0.15±0.04
	123.8		8.1±1.0	0.5 ±0.1
27.7/27.7	121.8	−20.2±1.5	10.1±1.0	0.4 ±0.3
42.0/25.3	91.6	−23.2±0.6	9.6±1.0	1.66±0.15
44.5/24.25	86.2	−22.0±0.8	8.9±0.9	1.78±0.20
48.3/22.4	78.0	−22.2±0.8	7.3±0.7	2.60±0.25
52.2/20.5	70.0	$-24.5^{+1.5}_{-2.5}$	7.4±0.7	2.9 ±0.3
56.0/18.25	60.8	$-27.0^{+2.0}_{-3,0}$	8.8±0.9	3.4 ±0.4
58.5/16.7	55.0	−19.1±2.0	7.0±0.7	4.0 ±0.4

The largest angle θ_{d*} at which the reaction p+d → p+p+n has been investigated is 152°. The corresponding experimental data are shown in fig. 4d. These data are compared with a calculation† based on ansatz (8). The result of the calculation is represented by the dashed curve of fig. 4d. The ansatz fits the data nearly along the whole kinematical curve, while the Watson calculation (solid curve) is only able to reproduce the FSI peak. The excellent agreement achieved with the impulse approximation is due to the different energy dependence of the two factors in formula (8). The first factor $|\psi_d|^2$ has its maximum at the minimum value of k_3^i. The minimum corresponds in fig. 4d to $S = 80$ MeV. The second factor the n–p cross section $(d\sigma/d\Omega)_{np}$ has a maximum at $E_{45} = 0$ corresponding to $S = 105$ MeV in fig. 4d. At low relative energies the spectator model is identical with the Watson model because the cross sections $(d\sigma/d\Omega)_{np}$ for neutron-proton singlet and triplet scattering are in very good approximation proportional to the enhancement factors F^s_{np} and F^t_{np} and the factor $|\psi_d|^2$ varies only slowly with energy in the region of FSI.

† The ratio of the singlet and triplet cross sections at $E_{np} = 0$ used in this first comparison was evaluated from the data in table 1. In general this ratio can be determined from the experimental data with formula (8), this will be discussed elsewhere.

After discussion of the more sophisticated treatment of the data taken at backward angles θ_{d^*} one of the aims of the whole set of experiments is to be recalled. The aim was to establish an angular distribution for the production of final state interacting n–p pairs with zero relative energy E_{np}. From the discussion given above it can be concluded that the Watson ansatz is very adequate for this purpose. Therefore the data measured at ten different pairs of angles were analysed in terms of eq. (7). The results obtained are summarized in table 1. The extracted n–p singlet scattering length is given together with the cross sections for the n–p singlet and triplet FSI at $E_{np} = 0$. The angular distribution of the singlet and triplet cross section are shown in fig. 7 and will be discussed in subsect. 3.2.2.

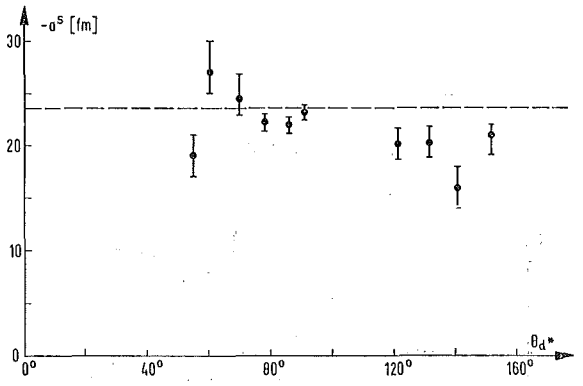

Fig. 6. The singlet n–p scattering length a^s obtained by analysing the three-particle cross-section at different angles θ_{d^*}. The dashed line indicates the scattering length known from free n–p scattering ($a^s = -23.68$ fm).

The scattering lengths obtained are plotted versus the production angle θ_{d^*} in fig. 6. The value of the free n–p scattering length $a^s = -23.68$ fm is indicated by a dashed line. Preliminary results have been already reported at the Birmingham conference [29])†. The best agreement with the free scattering length is obtained at production angles θ_{d^*} between 70° and 90°. As was already shown in the discussion of fig. 3 one expects the most reliable determination of a^s in this angular region, where the FSI is almost undisturbed by other contributing reaction mechanisms.

To check the consistency of the analysis the least-square fit calculations have been carried out taking into account different numbers of experimental points. The error flags shown in fig. 6 do not represent the statistical errors only but contain also the variation due to the different number of points used in the fit procedure. For production angles at about 80° the analysis is largely independent on the chosen number of points and the resulting error of a^s is small (see fig. 6). The mean value obtained for

† Contrarily to the present report the angle θ_{p3} has been used as abscissa and finite experimental resolutions had not yet been included.

the scattering length from the three measurements at $\theta_{d^*} = 78.0°$, 86.2°, 91.6° is $a^s = -22.7 \pm 0.5$ fm in good agreement with the value known from the free n–p scattering.

In general one has to be very careful with the extraction of the scattering length by using the simple Watson model. Accurate values will only be obtained at conditions where no other reaction mechanisms interfere with the FSI of the neutron-proton pair. At the c.m. energy of our experiments the purest FSI is observed near $\theta_{d^*} = 80°$, while at smaller or larger angles θ_{d^*} one finds considerable poorer agreement with the predictions of the Watson theory. This result is of specific interest in using the same procedure to determine the neutron-neutron scattering length [1–3]) from the reaction $n+d \rightarrow n+n+p$.

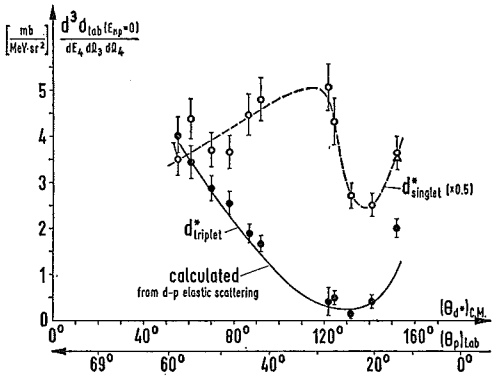

Fig. 7. The angular distribution of the three-particle cross section for the production of final state interacting singlet and triplet n–p pairs at relative energy $E_{np} = 0$. As abscissa the angle θ_{d^*} as well as the lab angle of the "free" proton θ_p^{lab} are chosen. The solid curve is the result of a calculation which connects the three particle cross section quantitatively with the cross section of elastic p–d scattering. The triangle denotes the prediction for the singlet cross section at the backward angle of $\theta_{d^*} = 152°$.

3.2.2. *Discussion of the angular distribution.* Fig. 7 shows the lab cross section at relative energy $E_{np} = 0$ for the production of n–p pairs in the singlet and triplet states (data from table 1). The cross sections are plotted in a linear scale as a function of the production angle θ_{d^*} of the low-energy n–p subsystem †. The angular distributions exhibit remarkably different shapes. The triplet cross section decreases monotonically to a minimum at $\theta_{d^*} = 130°$ subsequently it increases at backward angles. Contrarily the singlet contribution has a maixmum at $\theta_{d^*} \approx 110°$ which is followed by a steep decrease and a minimum at 140°.

Comparing the angular distribution of the triplet cross section with the cross section of elastic deuteron-proton scattering [27]) one observes a remarkable similarity of the

† An angular distribution for the three-particle cross section has been obtained in a less elaborate analysis where the singlet and triplet state contributions have not been separated [31]).

two distributions. The question arises whether the triplet angular distribution of the three-particle reaction can be understood with the knowledge of the elastic proton-deuteron scattering.

The quantitative relation to be deduced has to connect the reaction

$$p+d \rightarrow p+d^*_{triplet} \rightarrow p+p+n \tag{9a}$$

with

$$p+d \rightarrow p+d \text{ (elastic scattering)}. \tag{9b}$$

The main difference between these two reactions is that the neutron-proton system is produced in a bound ($Q = 0$ MeV) and an unbound ($Q = -2.224$ MeV) state respectively whereas the spin states of the bound deuteron and the triplet d* are identical.

The relation required has to connect the three-particle cross section $d^3\sigma/dE_4 d\Omega_3 d\Omega_4$ of reaction (9a) to the two-particle cross section $(d\sigma/d\Omega)_{elastic}$ of reaction (9b). Consequently the corresponding transition matrix elements have to be discussed. Taking into account the particle spins and the antisymmetrization of the wave functions the matrix element for the elastic p–d scattering can be written in the Born approximation in the following form

$$T_{fi}^{el} = (\psi_d e^{i\boldsymbol{k}''\cdot\boldsymbol{r}}\chi_f, \{1-PQ\}\{V_{pp}+V_{pn}\}\psi_d e^{i\boldsymbol{k}\cdot\boldsymbol{r}}\chi_i). \tag{10}$$

The matrix element for the three-particle reaction (9a) leading to the neutron-proton triplet FSI is given by

$$T_{fi}^{tripl} = (\psi_\kappa e^{i\boldsymbol{k}'\cdot\boldsymbol{r}}\chi_f, \{1-PQ\}\{V_{pp}+V_{pn}\}\psi_d e^{i\boldsymbol{k}\cdot\boldsymbol{r}}\chi_i), \tag{11}$$

where ψ_d and ψ_κ are the wave functions of the deuteron and of the n–p subsystem in the triplet state where κ is the relative momentum. The potential $(V_{pp}+V_{np})$ is the interaction potential between the incident deuteron and the target proton; $\boldsymbol{k}$ is the momentum of the proton in the entrance channel whereas $\boldsymbol{k}'$ and $\boldsymbol{k}''$ denote the momenta of the "free" proton in the inelastic and elastic exit channel respectively (see fig. 5a), χ_i and χ_f are the spinors of the initial and final state. The operators P and Q exchange the space and spin coordinates of the two protons.

Comparing the two matrix elements there is firstly a slight difference between the values $\boldsymbol{k}'$ and $\boldsymbol{k}''$ which is caused by the binding energy of 2.224 MeV of the deuteron. At our energy this off-energy-shell effect can be neglected and at identical production angles $\theta_d = \theta_{d^*}$ the vector $\boldsymbol{k}'$ is taken to be equal to $\boldsymbol{k}''$.

Secondly there is a difference between the wave function of the deuteron and the wave function of the n–p pair in the FSI triplet state. The radial parts $u = \text{const}\, r\psi(r)$ of the wave functions were calculated for the deuteron and for a free n–p pair with $E_{np} = 0$ keV. A square well potential with parameters which reproduce the neutron-proton scattering length and the effective range [43]) was used. Fig. 8 shows the potential parameters and the two wave functions normalized to $u(r) = 1$ at their maximum value.

Within the range of the potential the two wave functions have nearly the same radial dependence. The differences are small because the free n–p pair is taken to be produced with a relative energy $E_{np} = 0$ and the deuteron binding energy is small compared with the potential depth $V = 35.3$ MeV. Therefore inside the potential well the shapes of the two wave functions are regarded as identical.

Outside the range of the potential the two wave functions are very different. By discussion of all the graphs given in fig. 5a it has been shown in ref. [44]) that the integrals over the internal coordinates of the deuteron and of the n–p pair are only slightly affected by the shape of the wave functions outside the range of the n-p potential pro-

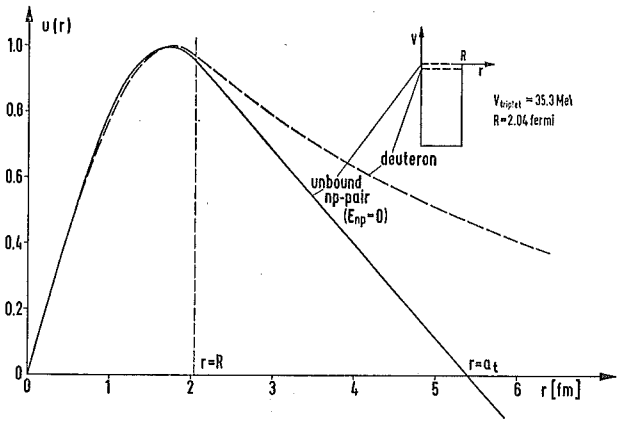

Fig. 8. Radial part of the deuteron wave function and the wave function of the unbound n–p pair in the triplet state at a relative energy $E_{np} = 0$. The parameters of the square well potential used are given.

vided the total energy in the three-particle c.m. system is large compared with the binding energy of the deuteron. Therefore contributions from outside the potential range can be neglected.

Assuming a large c.m. energy and a low relative energy E_{np} the ratio of the matrix elements is given by

$$\frac{|T_{fi}^{tripl}|^2}{|T_{fi}^{el}|^2} = \frac{|\psi_\kappa(r=0)|^2}{|\psi_d(r=0)|} \equiv \Phi(E_{np}), \tag{12}$$

where $\psi_\kappa(r = 0)$ and $\psi_d(r = 0)$ denote the values of the wave functions at the origin. In a good approximation $\Phi(E_{np})$ is proportional to the Watson enhancement factor F_{np}^t as defined by eq. (4).

The square of the ratio of the wave functions $\psi_\kappa(r = 0)$ and $\psi_d(r = 0)$ was evaluated at zero relative energy to be $\Phi(E_{np} = 0) = 5.45 \times 10^{-37}$ cm^3. This value was obtained by using the Hulthén wave function [42]) for the deuteron and the continuum

wave function for the n–p pair as given by Gammel *et al.* [41]). The three-particle cross section is given by

$$\frac{\mathrm{d}^3\sigma_{\mathrm{tripl}}}{\mathrm{d}E_4\,\mathrm{d}\Omega_3\,\mathrm{d}\Omega_4} = \frac{\rho_3}{\rho_2}\,\Phi(E_{\mathrm{np}})\left(\frac{\mathrm{d}\sigma}{\mathrm{d}\Omega}\right)_{\mathrm{elastic}}, \tag{13}$$

where ρ_2 and ρ_3 are the phase space factors for the reactions (9b) and (9a). The full curve of fig. 7 was calculated using eq. (13) at $E_{\mathrm{np}} = 0$ and the data of the elastic proton-deuteron scattering at $E_{\mathrm{d}} = 51.5$ MeV [ref. [27])]. A very good agreement between the experimental data and the calculated curve is observed. The absolute magnitude as well as the angular dependence are surprisingly well reproduced.

It should be noticed that Gell-Mann and Watson [45]) have discussed a very similar question dealing with the interaction between π-mesons and nucleons. They have compared the cross sections of the reactions

$$\mathrm{p+p} \rightarrow \pi^+ + \mathrm{n+p}, \tag{14a}$$

$$\mathrm{p+p} \rightarrow \pi^+ + \mathrm{d}, \tag{14b}$$

accounting for the production of n–p pairs in the isosinglet state $T = 0$. The cross sections of the two reactions were connected by an expression which is formally identical with eq. (13). The relation was deduced from the general arguments of the Watson model [45,46]). In lack of extensive experimental data especially for the three-particle break-up reaction the relation was confirmed only within 50 % for the reactions (14a) and (14b). The reason for this result might partially be due to the fact that the comparison was based on experimental data which contained already an integration over a wide kinematical region.

Discussing the $J_2^{\pm}$ type of the graphs only Frank and Gammel have derived a relation between the three-particle and the two-particle reaction cross sections [41]). These authors conclude that the triplet and the singlet angular distribution should have the same shape. This prediction is in contradiction to our experimental results. In a more sophisticated treatment all the three types of graphs have to be discussed as is shown in ref. [44]).

The successful application of relation (13) proves that this formula can be regarded to be a widely generalized form of the Watson FSI formula. The absolute value of the three-particle cross section can be evaluated from formula (13) as a function of the relative energy E_{np}, the c.m. energy and the production angle of the n–p pair. In general the singlet neutron-proton FSI cannot be predicted from the elastic proton-deuteron scattering. Due to the spin dependence of the nuclear forces the singlet state is not comparable to the n–p triplet bound state (deuteron) and a bound singlet state of the neutron-proton system does not exist. The n–p singlet FSI and the elastic p–d scattering may be simply related at backward angles ($\theta_{\mathrm{d}^*} > 140°$) only. The contributions of the graphs $J_2^{\pm}$ dominate at these backward angles (see fig. 5b). A ratio of the cross sections of n–p singlet and n–p triplet FSI can be predicted by using the

relation for quasielastic n–p scattering (8). For zero relative energy one obtains

$$\frac{\mathrm{d}^3\sigma_{\text{singlet}}}{\mathrm{d}E_4\,\mathrm{d}\Omega_3\,\mathrm{d}\Omega_4} \Big/ \frac{\mathrm{d}^3\sigma_{\text{triplet}}}{\mathrm{d}E_4\,\mathrm{d}\Omega_3\,\mathrm{d}\Omega_4} = \frac{1}{3}\left(\frac{a^s}{a^t}\right)^2, \tag{15}$$

where a^s and a^t are the scattering lengths for n–p singlet and triplet scattering. The three-particle cross section of n–p singlet FSI was calculated for $\theta_{d^*} = 152°$ and $E_{np} = 0$ by use of the expressions (13) and (15)

$$\frac{\mathrm{d}^3\sigma_{\text{singlet}}}{\mathrm{d}E_4\,\mathrm{d}\Omega_3\,\mathrm{d}\Omega_4} = 7.1\left[\frac{\text{mb}}{\text{MeV}\cdot\text{sr}^2}\right].$$

This value is shown in fig. 7 as a triangle. A very good agreement with the experimental result given in table 1 and fig. 7 is obtained.

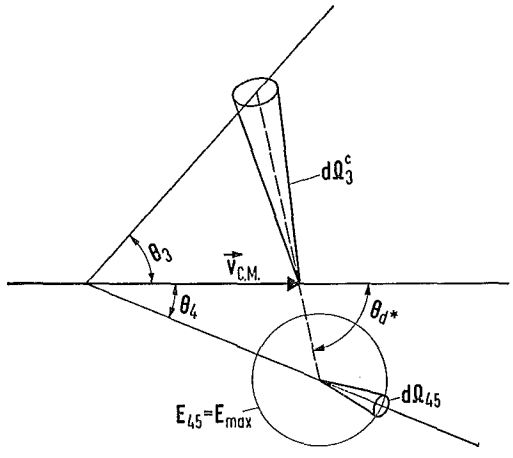

Fig. 9. Definition of the solid angles in the three-particle c.m. system and in the c.m. system of the n–p subsystem. The notation is used in eq. (16).

A quite different point to be discussed concerns the ratio of the number of elastically scattered deuterons to the total number of final state interacting n–p pairs which are produced at a fixed angle θ_{d^*} (at the same conditions in the entrance channel). To evaluate the total number of neutron-proton pairs one has to integrate over the internal angular and momentum coordinates of the neutron-proton subsystem. Carrying out this integration separately for the singlet and triplet n–p pairs one obtains the c.m. cross section $\mathrm{d}\sigma/\mathrm{d}\Omega_3^c$ of the singlet and triplet FSI. These integral cross sections are directly comparable with the elastic deuteron-proton cross section $(\mathrm{d}\sigma/\mathrm{d}\Omega)_{\text{elastic}}$

The lab three-particle cross section was transformed into the recoil c.m. system for the n–p pair [see for notation fig. 9 and e.g. ref. [36])]. Subsequently the integration was carried out over the solid angle Ω_{45} and the relative energy E_{45} of the neutron-proton subsystem. The d* system was assumed to be produced in a pure S-state corresponding to an isotropic n-p angular distribution.

The integrated cross section is

$$\frac{d\sigma}{d\Omega_3^c} = \left(\frac{d\sigma}{d\Omega_3^c}\right)_{\text{singlet}} + \left(\frac{d\sigma}{d\Omega_3^c}\right)_{\text{triplet}}$$

$$= \int_0^{E_{\max}} \int_{-\pi}^{\pi} \int_0^{2\pi} \frac{d^3\sigma}{dS\, d\Omega_3\, d\Omega_4} \frac{\partial(S, \Omega_3, \Omega_4)}{\partial(E_{45}, \Omega_3^c, \Omega_{45})} dE_{45}\, d\Omega_{45}. \qquad (16a)$$

Using eq. (5) one obtains for the FSI of the n–p pair (4, 5)

$$\frac{d\sigma}{d\Omega_3^c} = 4\pi \left[X_{np}^s(\theta_3) \int_0^{E_{\max}} F_{np}^s(E_{45}) \rho(E_{45}) dE_{45} + X_{np}^t(\theta_3) \int_0^{E_{\max}} F_{np}^t(E_{45}) \rho(E_{45}) dE_{45} \right].$$

The integration can be carried out easily because the phase space factor $\rho(E_{45})$ in the c.m. system as well as the enhancement factor of the Watson ansatz is independent on the angular coordinates of the n–p subsystem (4, 5). The values of X_{np}^s, X_{np}^t and a^s were already determined by the least-square fit calculations discussed in subsect. 3.2.1.

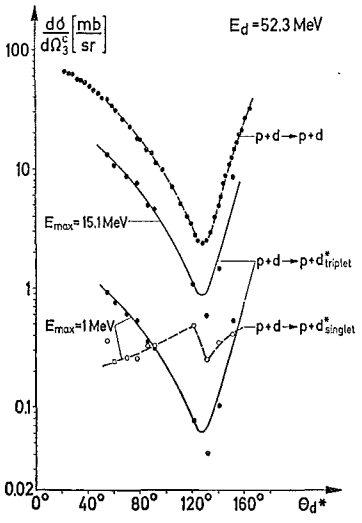

Fig. 10. The angular distribution of the c.m. cross section for neutron-proton singlet and triplet FSI obtained by integration of the three-particle cross section. For comparison the cross section of elastic p–d scattering (27) is also shown.

The total number of neutron-proton triplet and singlet FSI pairs would be obtained by integrating up to the maximum energy available in the recoil c.m. system. In our experiment this energy is $E_{\max} = E_{\text{c.m.}} = 15.1$ MeV. An integration up to the maximum energy implies the validity of the enhancement factor $F_{np}(E_{np})$ at relative energies of up to 15.1 MeV. The Watson model, however, should surely not be extended to such high relative energies. Consequently the same integration has been carried out

restricting only the limit to an arbitrary lower value of $E_{max} = 1$ MeV. Up to this energy the Watson ansatz surely can be used.

Fig. 10 shows the c.m. cross sections for neutron-proton singlet and triplet FSI integrated up to $E_{max} = 1$ MeV. The result of an integration up to 15.1 MeV is only shown for the neutron-proton triplet state because the high-energy region does not contribute appreciably to the singlet cross section. The angular distribution of the elastic deuteron-proton scattering [27]) is also given in fig. 10. The similarity between the angular distribution of the elastic deuteron-proton scattering and the neutron-proton triplet FSI is obvious. For ease of comparison two curves are shown which were obtained by multiplying the elastic cross section by a properly chosen constant factor. The experimental data for the singlet neutron-proton FSI are connected by a dashed line and exhibit a singificantly different angular distribution.

3.2.3. *Proposed generalization of the results obtained to cluster phenomena.* The three-particle differential cross section of the triplet neutron-proton FSI (fig. 7) predicted with the knowledge of the elastic proton-deuteron scattering is in excellent agreement with the experimental results. For the reaction studied which is discussed in subsect. 3.2.2 the wave functions of the bound deuteron and the triplet neutron-proton pair were known. By generalizing the validity of the method discussed above one might think of an extension of the procedure to such composite systems where information on the wave function is needed.

An example is ^{6}Li where one wants to detrmine the probability for the d–α cluster configuration. Such a cluster probability might be measured by investigating the elastic scattering

$$\alpha + {}^6\mathrm{Li} \rightarrow \alpha + {}^6\mathrm{Li}$$

and the d–α final state interaction in the break-up reaction

$$\alpha + {}^6\mathrm{Li} \rightarrow \alpha + (\mathrm{d} + \alpha).$$

The energy necessary for the break-up of the ^{6}Li nucleus into an α-particle and a deuteron is 1.5 MeV only. This binding energy is small compared to the interaction potential. Accordingly at $E_{\alpha d} = 0$ the wave functions for the bound state and the final state interacting d–α pair should have nearly the same shape inside the interaction potential, as long as ^{6}Li is considered to be a pure d–α cluster in the S-state.

Experimental data should answer the question whether the two angular distributions are similar and whether the absolute values of the break-up cross sections can be predicted from the elastic α–^{6}Li scattering. Such an analysis should be able to reveal the d–α cluster probability. If a ^{3}He-triton cluster configuration were dominating a different angular distribution would be observed. The procedure proposed might be advantageous compared to investigations by means of the quasielastic scattering because it accounts for all interactions between the projectile particle and the cluster constituents.

4. Conclusion

The experimental results discussed above can be taken as a proof of the applicability of the two-step reaction model. This conclusion is to be drawn from two different aspects. Firstly the two-nucleon scattering parameter a^s extracted from the three-particle reaction turns out to be in good agreement with the value known from free n–p scattering. For a specific kinematic situation the agreement is excllent but even in the whole kinematical region investigated the overall agreement is very good. Secondly the angular distribution for the production of zero energy n–p pairs in the triplet state shows the same shape like the angular distribution of elastic p–d scattering. This result is easily explained by the two-step reaction model. The absolute comparison of these two angular distributions yields a very good quantitative explanation by accounting only for graphs of the two-step type.

In addition to the experiments discussed above a measurement of the n–p angular distribution in the c.m. of the n–p subsystem should verify the reliability of the two-step reaction model. If the two reaction steps proceed independently one expects the d* production probability to be independent of all variables in the n–p subsystem. Such experiments have been carried out and will be reported separately.

At backward scattering angles θ_{d*} in the three-particle c.m. system the two-step reaction mechanism reduces to a one-step reaction mechanism. The experimental result is best explained by the use of the impulse approximation. At these special kinematical conditions the impulse approximation turns out to be a generalization of the Watson ansatz.

The authors want to express their gratitude to Prof. Dr. A. Citron, Prof. Dr. W. Heinz and Prof. Dr. H. Schopper for their encouragement and support. We are indebted to Dr. H. D. Zeh for many very valuable discussions concerning the theoretical interpretation of the experimental results. We would like to thank Dr. F. K. Schmidt, W. Gehrke and R. Schlüfter for their assistance in the experiment. The good cooperation of Dr. G. Schatz and the members of the cyclotron staff is gratefully acknowledged.

References

1) B. Zeitnitz, R. Maschuw and P. Suhr, Phys. Lett. **28B** (1969) 420; DESY Report 70/7 (1970)
2) C. Perrin, J. S. Gondrand, M. Durand, S. Desreumaux and R. Bouchez, Proc. of the Conf. on the three-body problem, Birmingham, 1969, p. 26
3) A. Grässler and R. Honecker, Nucl. Phys. **A136** (1969) 446
4) L. D. Faddeev, JETP (Sov. Phys.) **12** (1961) 1014
5) C. Lovelace, Phys. Rev. **135** (1964) B1225
6) A. C. Phillips, Phys. Rev. **142** (1966) 984, **145** (1966) 733
7) E. O. Alt, P. Grassberger and W. Sandhas, Nucl. Phys. **B2** (1967) 167
8) P. Grassberger and W. Sandhas, Nucl. Phys. **B2** (1967) 181
9) E. O. Alt, P. Grassberger and W. Sandhas, Phys. Rev. **C1** (1970) 85
10) L. M. Delves and A. C. Philips, Rev. Mod. Phys. **41** (1969) 497

11) A. Aaron, R. D. Amado and Y. Y. Yam, Phys. Rev. **140** (1965) B1291, **150** (1966) 857
12) R. T. Cahill and I. H. Sloan, Proc. of the Conf. on the three-body problem, Birmingham, 1969 (North-Holland, Amsterdam, 1970) p. 265
13) W. T. H. van Oers, preprint of the University of Winitoba, Winnipeg, Canada (1968)
14) W. T. H. van Oers and I. Šlaus, Phys. Rev. **160** (1967) 853
15) I. Šlaus, J. W. Verba, J. R. Richardson, R. F. Carlson and L. S. August, Phys. Lett. **23** (1966) 358
16) I. Šlaus, Proc. of the Conf. on the three-body problem, Birmingham, 1969, p. 337
17) A. Niiler, C. Joseph, V. Valković, W. von Witsch and G. C. Phillips, Phys. Rev. **182** (1969) 1083
18) R. J. Griffiths and K. M. Knight, Nucl. Phys. **54** (1964) 56
19) D. P. Boyd, P. F. Donovan and J. F. Mollenauer, preprint of the Rutgers State University, 1968
20) J. Arvieux, J. L. Durand, A. Papineau and A. Tarrats, Proc. of the Conf. on the three-body problem, Birmingham, 1969 (North-Holland, Amsterdam, 1970) p. 212
21) M. L'Huillier, N. Marty, M. Morlet, B. Tatischeff and A. Willis, Proc. of the Conf. on the three-body problem, Birmingham, 1969 (North-Holland, Amsterdam, 1970) p. 430
22) W. J. Braithwaite, J. M. Cameron, D. W. Storm, D. J. Margaziotis, G. Paić, J. G. Rogers, J. W. Verba and J. C. Young, Proc. of the Conf. on the three-body problem, Birmingham, 1969 (North-Holland, Amsterdam, 1970) p. 407
23) A. F. Kuckes, R. Wilson and P. F. Cooper, Ann. of Phys. **15** (1961) 193
24) B. Kühn, H. Kumpf, K. Möller and J. Mösner, Nucl. Phys. **A120** (1968) 285
25) H. Jeremie and T. Grandy, Nucl. Phys. **A132** (1969) 571
26) W. D. Simpson, W. R. Jackson and G. C. Phillips, Nucl. Phys. **A103** (1967) 97
27) H. Brückmann, W. Kluge and L. Schänzler, Z. Phys. **217** (1968) 305
28) H. Brückmann, W. Gehrke, W. Kluge, H. Matthäy, L. Schänzler and K. Wick, report of the Kernforschungszentrum Karlsruhe KFK 892 (1968)
29) H. Brückmann, W. Gehrke, W. Kluge, H. Matthäy, L. Schänzler and K. Wick, Proc. of the Conf. on the three-body problem, Birmingham, 1969, p. 230; Report of the Kernforschungszentrum Karlsruhe KFK 1012 (1969)
30) H. Brückmann, W. Kluge, H. Matthäy, L. Schänzler and K. Wick, Phys. Lett. **30B** (1969) 460
31) H. Brückmann, W. Gehrke, W. Kluge, H. Matthäy, L. Schänzler and K. Wick, Z. Phys. **235** (1970) 453; report of the Kernforschungszentrum Karlsruhe KFK 1130 (1970)
32) K. M. Watson, Phys. Rev. **88** (1952) 1163
33) A. B. Migdal, ZhETF **28** (1955) 3
34) H. Brückmann, E. L. Haase, W. Kluge and L. Schänzler, Nucl. Instr. **67** (1969) 29
35) H. Brückmann, report of the Kernforschungszentrum Karlsruhe KFK 912 (1968);
H. Brückmann, P. Fluck, H. Matthäy and L. Schänzler, report of the Kernforschungszentrum Karlsruhe KFK 897 (1968)
36) G. G. Ohlsen, Nucl. Instr. **37** (1965) 240
37) G. F. Chew and F. E. Low, Phys. Rev. **113** (1959) 1640
38) M. C. Goldberger and K. M. Watson, Collision theory (Wiley, New York, 1964) p. 479
39) H. P. Noyes, Phys. Rev. **130** (1963) 2025
40) R. L. Gluckstern and H. A. Bethe, Phys. Rev. **81** (1951) 761
41) R. M. Frank and J. L. Gammel, Phys. Rev. **93** (1954) 463
42) R. S. Christian and J. L. Gammel, Phys. Rev. **91** (1953) 100
43) G. L. Squires, Progr. Nucl. Phys. **2** (1953) 89
44) K. Wick, Ph.D. thesis, University of Karlsruhe (1970)
45) M. Gell-Mann, K. M. Watson, Ann. of Nucl. Sci. **4** (1954) 219
46) K. M. Watson, Phys. Rev. **88** (1952) 1163